

AUTOMATIC EXUDATES DETECTION FROM DIABETIC RETINOPATHY RETINAL IMAGE USING FUZZY C-MEANS AND MORPHOLOGICAL METHODS

Akara Sopharak¹, Bunyarit Uyyanonvara²

^{1,2}Sirindhorn International Institute of Technology, Thammasat University
131 Moo 5, Tiwanont Road, Bangkadi, Muang, Pathumthani 12000
Thailand

¹akara@siit.tu.ac.th, ²bunyarit@siit.tu.ac.th

ABSTRACT

Exudates are the primary signs of diabetic retinopathy which are mainly cause of blindness and could be prevented with an early screening process. Pupil dilation is required in the normal screening process but this affects patients' vision. This paper investigated and proposed automatic methods of exudates detection on low-contrast images taken from non-dilated pupils. The process has two main segmentation steps which are coarse segmentation using Fuzzy C-Means clustering and fine segmentation using morphological reconstruction. Four features, namely intensity, standard deviation on intensity, hue and adapted edge, were selected for coarse segmentation. The detection results are validated by comparing with expert ophthalmologists' hand-drawn ground-truth. The sensitivity and specificity for our exudates detection are 86% and 99% respectively.

KEY WORDS

Exudates, diabetic retinopathy, non-dilated retinal images, and Fuzzy C-Means

1. Introduction

Blindness is an outcome of diabetic retinopathy and its prevalence is set to continue rising. Estimated 50-65 new cases of blindness per 100,000 happened every year [1]. The screening of diabetic patients for the development of diabetic retinopathy can potentially reduce the risk of blindness in these patients by 50% [2-6]. An early detection enables laser therapy to be performed to prevent or delay visual loss and may be used to encourage improvement in diabetic control. Current methods of detection and assessment of diabetic retinopathy is manual, expensive and require trained ophthalmologists. In this paper, we present automatic exudates detection in order to detect and treat diabetic retinopathy in an early stage.

G.G. Gardner *et al.* [7] proposed an automatic detection of diabetic retinopathy using an artificial neural network.

The exudates are identified from grey level images. The fundus image was analyzed using a back propagation neural network. This was the result of classifying the whole 20x20 region rather than a pixel-level classification. C. Sinthanayothin *et al.* [8] reported the result of an automated detection of diabetic retinopathy on digital fundus image by Recursive Region Growing Segmentation (RRGS) algorithm on 10x10 window. Wang *et al.* [9] used colour features on Bayesian statistical classifier to classify each pixel into lesion or non-lesion classes. Walter *et al.* [10] detected exudates using grey level variation and means of morphological reconstruction techniques. Osareh *et al.* [2, 11-13] used colour normalization, local contrast enhancement in pre-processing step. The colour retinal images is segmented using Fuzzy C-Means (FCM) clustering and then classify the segmented regions into two disjoint classes, exudates and non-exudates patches using neural network. The feature set used for training the neural network are size, colour, average intensity, edge sharpness and standard deviation of intensity. They also locate the optic disc using snakes. Xiaohui Zhang and Chutatape Opas [14] used Improved FCM (IFCM) to segment candidate bright lesion areas. Then a hierarchical Support Vector Machines (SVM) classification structure is applied to classify bright non-lesion areas.

Most of techniques mentioned earlier worked on dilated pupils which the exudates and other retinal features are clearly visible. In normal diabetic retinopathy screening process, pupils were dilated using Tropicamide 1% eye drop. The process takes about 15-20 minutes to work and have an effect to patient. The dilating drops may impair focusing of the eyes for several hours and produce a brief stinging sensation, nausea, vomiting, dryness of the mouth and dizziness. The examination time and patient's effect could be reduced if the system can work on non-dilated pupil. Therefore, this paper proposed exudates detection on retinal images and low quality images from non-dilated pupils.

2. Methodology

All digital retinal images of patient's non-dilated pupils were obtained from KOWA-7 non-mydratic retinal camera with a 45° field of view taken at Thammasat hospital. The images were stored in a JPEG image format (.jpg) files with lowest compression rates. The image size is 500 x 752 pixels at 24 bit.

Firstly, the raw images were processed using a pre-processing method described in 2.1, in order to get the contrast of the image enhanced and ready for the next step. In section 2.2, methods for exudates detection is explained.

2.1 Preprocessing

Firstly, original image's Red, Green and Blue (RGB) space was transformed to Hue, Saturation and Intensity (HSI) space. A median filtering operation was then applied on this I band to reduce noise before a Contrast-Limited Adaptive Histogram Equalization (CLAHE) [15] was applied for contrast enhancement. CLAHE operates on small regions in the image. Each small region's contrast is enhanced with histogram equalization. Original intensity band image and intensity bands after preprocessing are shown in Fig. 1 (a) and Fig. 1 (b), respectively.

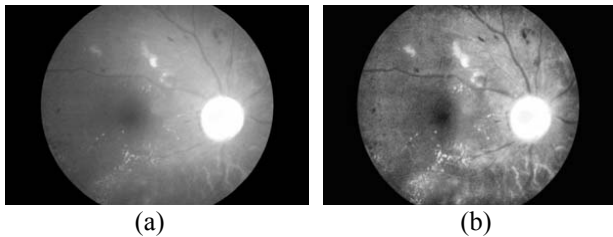


Figure 1. Pre-processing result (a) Original I band, (b) I band after pre-processing.

2.2 Detecting Exudates

The exudates can be identified on the ophthalmoscope as areas with hard white or yellowish colours and varying sizes, shapes and locations, near the leaking capillaries within the retina. Main cause of exudates is proteins and lipids leaking from the blood into the retina via damaged blood vessels [2]. This paper proposed two main segmentation steps. The first step is coarse segmentation using FCM clustering and the second step is fine segmentation using morphological reconstruction.

2.2.1 Features Selection

Four features were selected as input for clustering in FCM. They are intensity image after pre-processing,

standard deviation of intensity image, hue image and adapted edge. Detail of each feature is described below.

1. Intensity image after pre-processing (I_{CLAHE}) is selected because exudates pixels could be distinguished by their intensity.

2. Standard deviation of I_{CLAHE} (Std) is also chosen because the distribution measurement of the data would differentiate the exudates area from the others since standard deviation shows the main characterization of the closely distributed cluster of exudates. Standard deviation is defined as Eq. (1).

$$Std(x) = \frac{1}{N-1} \cdot \sum_{i \in W(x)} (I_{CLAHE}(i) - \mu_{I_{CLAHE}}(x))^2 \quad (1)$$

where x is a set of all pixels in a sub-window $W(x)$, N is a number of pixels in $W(x)$, $\mu_{I_{CLAHE}}(x)$ is the mean value of $I_{CLAHE}(i)$ and $i \in W(x)$. Window size of 15 x 15 was used in this step.

3. Hue image is also a selected feature because hue components make up chrominance or colour information. Exudates appear differently in yellowish or white colour.

4. Because exudates have strong edge, we experimented by adding the edge pixels as one of the classification features. However, this edge feature needed preprocessing as follows:

4.1 For a quick edge calculation, Sobel operator of size 3x3 was used to compute the gradient magnitude.

4.2 The previous result was thresholded because the exudates areas usually have quite a strong edge.

4.3 Some of the strong edge pixels from the previous step are not totally edge of the exudates. Some of them are a part of vessel's edge. These vessel edge pixels need to be removed as many as possible in this step. Quick blood vessels detection was achieved by using decorrelation stretch on red band. The decorrelation stretch [18] is a process that is used to enhance or stretch the colour differences found in a colour image. The method used to do this includes the removal of the inter-channel correlation found in the input pixels. This is done by first finding the linear transformation that result in removing the correlation among the vectors in the transformed space. Result of blood vessel detection was shown in Fig. 2.

4.4 Few exudates are soft exudates which can not be detected by strong edge. We then have to add red pixels which were selected from decorrelation stretch image in previous result image because the soft exudates normally appears red.

4.5 However, the selected red pixels may include the region of optic disc. These red pixels which belong to optic disc have to be removed first. The optic disc was roughly detected by using entropy feature on I_{CLAHE} . The entropy is a statistic measure of

randomness that can be used to characterize the texture of the input image. Entropy is defined as Eq. (2).

$$H(x) = - \sum_{i \in W(x)} p_i \cdot \log_2(p_i) \quad (2)$$

where x is a set of all pixels in a sub-window $W(x)$, p_i is the histogram counts in sub-window and $i \in W(x)$. Window size that we used was 9×9 pixels.

In this step, in order to get rid of all regions with low local variation, the resulting image was thresholded at automatically selected grey level, using Otsu algorithm. To ensure that all the neighbouring pixels of the thresholded result were also included in the candidate region, binary dilation operator was also applied. This step, a flat disc-shaped structuring element with a fixed radius of eleven was used. Result from entropy technique and all optic disc area in the original image was masked out as shown in Fig. 3 (a) and Fig. 3 (b), respectively.

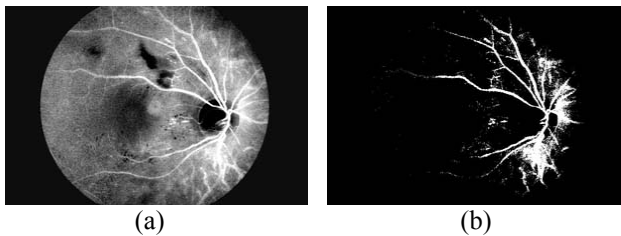


Figure 2. Blood vessel detection (a) Decorrelation stretch image on red plane (b) Blood vessel detected from decorrelation stretch image.

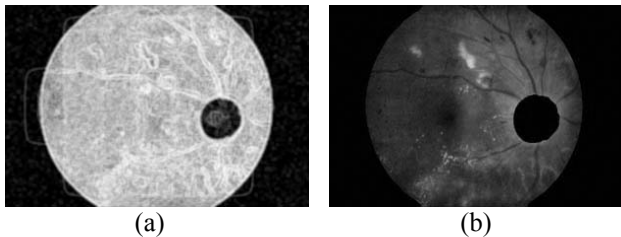


Figure 3. Optic disc detection (a) Entropy image, (b) Optic disc area eliminated from the contrast enhanced image.

4.6 A number of neighboring white pixels of the resulting image from process 4.1 – 4.5 was counted using window size of 17×17 to form our final feature, namely adapted edge as shown in Fig. 4 (d).

Image of four features are shown in Fig. 4. These four features were used to cluster retinal image into four clusters as described in the next section.

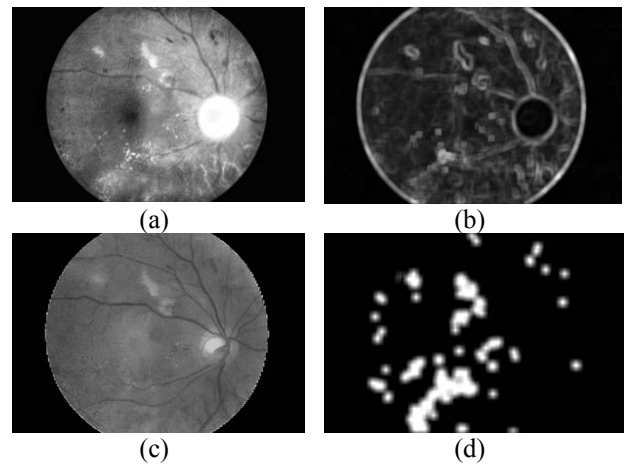


Figure 4. Input features for FCM clustering (a) Intensity image after pre-processing, (b) Standard deviation of intensity image, (c) Hue image, (d) Adapted edge image

2.2.2 Coarse Segmentation using Fuzzy C-Means Clustering

FCM clustering [14, 16, 17] is an overlapping clustering algorithm, each point may belong to two or more clusters with different degrees of membership. In this case, data will be associated to an appropriate membership value. It is based on minimization of the following objective function (Eq. 3).

$$J = \sum_{i=1}^N \sum_{j=1}^C u_{ij}^2 \|x_i - c_j\|^2 \quad (3)$$

where N is number of features, 4 for our case. C is number of clusters, also 4. u_{ij} is the degree of membership of x_i in the cluster j , x_i is the i th of d -dimensional measured data, c_j is the d -dimension center of the cluster, and $\|*\|$ is any norm expressing the similarity between any measured data and the center.

Fuzzy partitioning is carried out through an iterative optimization of the objective function shown above, with the update of membership u_{ij} and the cluster centers c_j by using Eq. 4 and Eq. 5, respectively.

$$u_{ij} = \frac{1}{\sum_{k=1}^C \left(\frac{\|x_i - c_j\|}{\|x_i - c_k\|} \right)^2} \quad (4)$$

$$c_j = \frac{\sum_{i=1}^N u_{ij}^2 x_i}{\sum_{i=1}^N u_{ij}^2} \quad (5)$$

This iteration will stop when Eq. (6) is satisfied.

$$\max_{ij} \left\{ \left| u_{ij}^{(k+1)} - u_{ij}^{(k)} \right| \right\} < \varepsilon \quad (6)$$

where ε is a termination criterion, 0.00001 for our case. k is the maximum iteration step, 200 for our case. This procedure converges to a local minimum or a saddle point of J . The algorithm is composed of the following steps:

<ol style="list-style-type: none"> 1. Initialize $U=[u_{ij}]$ matrix, $U^{(0)}$ 2. At k-step: calculate the centers vectors $C^{(k)}=[c_j]$ with $U^{(k)}$ $c_j = \frac{\sum_{i=1}^N u_{ij}^2 x_i}{\sum_{i=1}^N u_{ij}^2}$ 3. Update $U^{(k)}, U^{(k+1)}$ $u_{ij} = \frac{1}{\sum_{k=1}^c \left(\frac{\ x_i - c_j\ }{\ x_i - c_k\ } \right)^2}$ 4. If $\ U^{(k+1)} - U^{(k)}\ < \varepsilon$ then STOP; otherwise return to step 2.
--

The result from FCM clustering is shown Fig. 5. The result candidate exudates areas from FCM clustering are also shown in Fig. 6 (a).

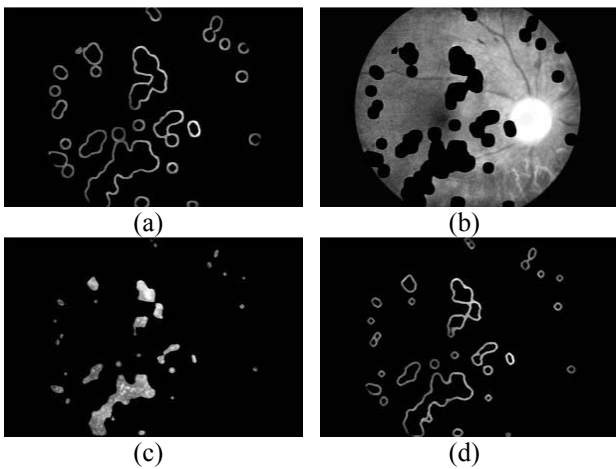


Figure 5. FCM clustering results (a) Cluster 1, (b) Cluster 2, (c) Cluster 3, (d) Cluster 4.

2.2.3 Fine Segmentation using Morphological Reconstruction

The result from the previous section was a rough estimation of the exudates. In order to get a better result, a fine segmentation using morphological reconstruction was applied in this step. Morphology reconstruction is a part of morphological image processing. Morphological reconstruction is based on dilation on two images, a marker and a mask.

The resulting image from coarse segmentation was used as a marker while original intensity image (f_i) was used as a mask. All the pixels in the marker were inverted before they were overlaid on the original image. The result, ex_1 , is shown in Fig. 6 (b). The morphological reconstruction by dilation, R , was then applied on the previous overlaid image using Eq. (7). The dilations of marker image under mask image were repeated until the contour of marker image fits under the mask image. The result is displayed in Fig. 6 (d).

$$ex_2(x) = R_{f_i}(ex_1) \quad (7)$$

Using Eq. (8), the final result is obtained by applying a threshold operation at automatically selected grey level α_1 to the difference between the original image (f_i) and the reconstructed image (ex_2). The resulting image is shown in Fig. 6 (e).

$$E_{seg} = T_{\alpha_1}(f_i - ex_2) \quad (8)$$

3. Result

Performance of our technique will be evaluated quantitatively by comparing the resulting of extractions with ophthalmologists' hand-drawn ground-truth images. This approach is to measure the correctness of the algorithms at the pixel level. This pixel-based evaluation considers four values are True Positive (TP), False Positive (FP), False Negative (FN) and True Negative (TN). From these quantities, the sensitivity was computed by $TP/TP+FN$ and specificity was also calculated by $TN/TN+FP$. Forty retinal images were processed by steps proposed in the methodology section. Time taken for running the whole process is 6 minutes per image. The sensitivity and specificity of the exudates detection that we received from this set of data are 86% and 99%, respectively.

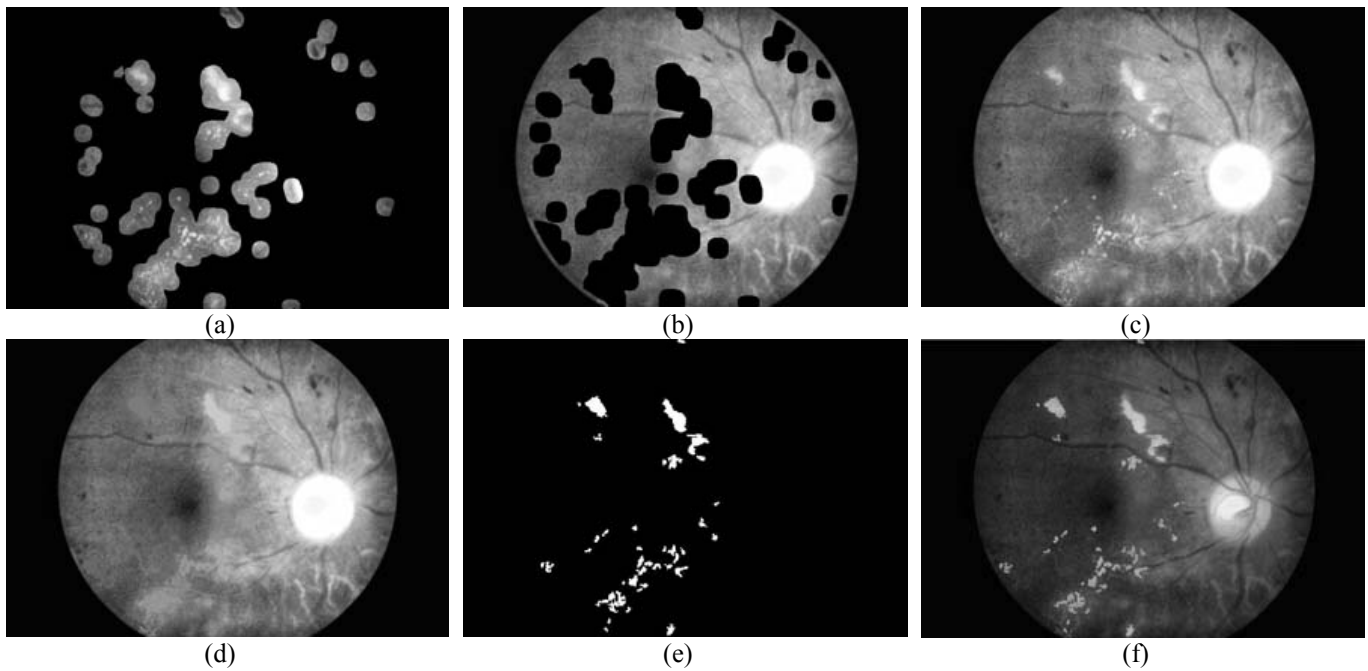


Figure 6. Exudates detection (a) Candidate areas after using Fuzzy C-Means clustering, (b) Marker image, (c) Mask image, (d) Reconstructed image, (e) Difference image, (f) Result superimposed on the original image.

4. Conclusion and discussion

In this work we have investigated and proposed exudates detection based on two segmentation techniques, namely, coarse segmentation using FCM clustering and fine segmentation using morphological reconstruction.

For FCM clustering, four input features based on characteristic of exudates were selected. These features are bright area, closely distributed cluster, white or yellowish colour and strong edge were used which are represented by intensity image, standard deviation of intensity image, hue image and adapted edge image respectively. Blood vessel and optic disc pixels were removed from the forth feature in order to prevent misclassification. However, the algorithm still has some false detection because some pixels with similar colour to the exudates belong to optic disc and edge of blood vessel.

The results demonstrated here indicate that the system can help the ophthalmologist to detect the exudates in the screening process. This research has not yet been utilized in real applications. The aim of further work is to improve the sensitivity value with lower false negative rate in order to give more accurate performance. Future work will address on finding effective characteristic of exudates which could distinguish them from other features (such as vessel and optic disc) of retinal image. These features may help reduce time consumption that this algorithm spent during vessel and optic disc detection. The detection time and misclassification of other features may lead to improvement of sensitivity and specificity values.

Acknowledgement

We would like to thank Eye Care Center, Thammasat hospital who supplied all the images used in this project.

References

- [1] J. A. Olson, F. M. Strachana, J. H. Hipwell, K. A. Goatman, K. C. McHardy, J. V. Forrester and P. F. Sharp, A comparative evaluation of digital imaging, retinal photography and optometrist examination in screening for diabetic retinopathy, *Diabetic Medicine*, 20(7), 2003, 528-534.
- [2] A. Osareh, M. Mirmehdi, B. Thomas and R. Markham, Automated Identification of Diabetic Retinal Exudates in Digital Colour Images, *British Journal of Ophthalmology*, 87(10), 2003, 1220-1223.
- [3] C. Sinthanayothin, J.F. Boyce, H.L. Cook, T.H. Williamson, Automated Localization of the Optic Disc, Fovea, and Retinal Blood Vessels from Digital Colour Fundus Images, *British Journal of Ophthalmology*, 83, 1999, 231-238.
- [4] C.I. Sanchez, R. Hornero, M.I. Lopez, J. Poza, Retinal Image Analysis to Detect and Quantify Lesions Associated with Diabetic Retinopathy, *Proc. 26th IEEE Annual International Conf. on Engineering in Medicine and Biology Society (EMBC)*, 3, 2004, 1624 – 1627.
- [5] W. Hsu, P.M.D.S Pallawala, Mong Li Lee, Kah-Guan Au Eong, The Role of Domain Knowledge in the Detection of Retinal Hard Exudates, *Proc. 2001 IEEE Computer Society Conf. on Computer Vision and Pattern Recognition*, 2, 2001, II-246 - II-251.

- [6] R. Paisan, W. Nattapon, S. Pattanaporn, P. Ekchai, T. Montip, Screening for Diabetic Retinopathy in Rural Area Using Single-Field, Digital Fundus Images, *Journal of Medical Association Thai*, 88, 2005, 176-180.
- [7] G.G. Gardner, D. Keating, T.H. Williamson, A.T. Elliot, Automatic Detection of Diabetic Retinopathy using an Artificial Neural Network: a Screening Tool, *British Journal of Ophthalmology*, 80, 1996, 940-944.
- [8] C. Sinthanayothin, J.F. Boyce, T.H. Williamson, H.L. Cook, Automated Detection of Diabetic Retinopathy on Digital Fundus Image, *International Journal of Diabetic Medicine*, 19, 2002, 105-112.
- [9] Wang, H., Hsu, W., Goh, K.G., Lee, An Effective Approach to Detect Lesions in Color Retinal Images, *Proc. IEEE Conf. on Computer Vision and Pattern Recognition*, 2, 2000, 181-186.
- [10] T. Walter, J.C. Klein, P. Massin, A. Erginay, A Contribution of Image Processing to the Diagnosis of Diabetic Retinopathy-Detection of Exudates in Colour Fundus Images of the Human Retina, *IEEE Transactions on Medical Imaging*, 21, 2002, 1236 - 1243.
- [11] A. Osareh, M. Mirmehdi, B. Thomas, and Richard Markham, *Medical image understanding and analysis* (BMVA Press, 2001).
- [12] A. Osareh, M. Mirmehdi, B. Thomas, and R. Markham, Classification and Localisation of Diabetic-Related Eye Disease, *7th European Conf. on Computer Vision*, 2002, 502-516.
- [13] A. Osareh, M. Mirmehdi, B. Thomas, and R. Markham, Comparative Exudate Classification using Support Vector Machines and Neural Networks, *The 5th International Conf. on Medical Image Computing and Computer-Assisted Intervention*, 2002, 413-420.
- [14] Xiaohui Zhang and Chutatape O, Top-down and bottom-up strategies in lesion detection of background diabetic retinopathy, *IEEE Computer Society Conf. on Computer Vision and Pattern Recognition (CVPR)*, 2, 2005, 422-428.
- [15] R.C. Gonzales, R.E. Woods, *Digital image processing* (Upper Saddle River, NJ: Addison-Wesley publishing Co., 2002).
- [16] X.Y. Wang, J. Garibaldi, and T. Ozen, Application of The Fuzzy C-Means clustering Method on the Analysis of non Pre-processed FTIR Data for Cancer Diagnosis, *Proc. of the ANZIS Conf.*, 2003, 233-238.
- [17] Musa H. Asyali, and Musa Alci, Reliability analysis of microarray data using fuzzy c-means and normal mixture modeling based classification methods, *Bioinformatics*, 21(5), 2005, 644-649.
- [18] Son Lam Phung, Abdesselam Bouzerdoum and Douglas Chai, Skin Segmentation Using Color Pixel Classification: Analysis and Comparison, *Proc. IEEE Transactions on Pattern Analysis and Machine Intelligence*, 27(1), 2005, 148 - 154.